Identification and Analysis of Spatio-temporal Dynamical Systems Using Wavelets

L. Z. Guo and S. A. Billings

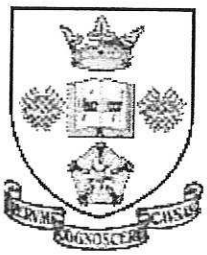

Department of Automatic Control and Systems Engineering
University of Sheffield
Sheffield, S1 3JD
UK

Research Report No. 869
August 2004

ıd analysis of spatio-temporal systems using wavelets

, L. Z. and Billings, S. A.

omatic Control and Systems Engineering
University of Sheffield
Sheffield S1 3JD, UK

Abstract

In this paper the identification and analysis of spatio-temporal dynamical systems is presented. An approximated B-spline wavelet representation of spatio-temporal dynamical systems is identified using an orthogonal least squares algorithm from measured data. Control variables are incorporated to represent controlled external inputs and/or some system parameters for the purpose of analysis. The identified system models can be used to evaluate how the external inputs or system parameters affect the evolution of the spatio-temporal dynamics and pattern formations. Two examples are used to illustrate the proposed approach.

1 Introduction

In recent years, increasing attention has been given to the analysis and control of the formation of spatio-temporal patterns. This involves a variety of fields such as physical, chemical, biological, ecological and engineering systems (Kaneko 1993, Sóle, Valls and Bascompte 1992, Yanagita and Kaneko 1997, Tabuchi, Yakawa and Mallick et al. 2002, Köhler, Reinhard and Huth 2002, Bertram, Beta, Rotermund, and Ertl 2003, Goldman, et al. 2003, Adamatzky 2003, Chen 1999). There are two important aspects in the study of spatio-temporal pattern formation and dynamics: one is to exploit the evolution of the underlying spatio-temporal dynamics under different external controlled inputs (this study may lead to the control problem for the spatio-temporal pattern formation), the other is to observe and analyse the influence of some of the parameters upon the behaviour of the systems (this study may lead to the analysis of nonlinear phenomena such as bifurcation, chaos etc.). However, both these problems can only be studied if a model of the system is known. But in practice this condition is often not met. In some instances, the dynamical origin of a spatio-temporal pattern formation can be obtained as a partial differential equation (PDE) either from *a priori* information or from a known analytical model. But even

when the PDE's are available from these sources they are often very simplified representations of the real dynamics. In many other cases, such as for example in ecological systems, only a series of snapshots of the spatial pattern are available. Therefore, it would be advantageous if a spatio-temporal model could be identified from the observed patterns. The model could then be used for the analysis of pattern formation or for control.

Various methods for the identification of local CML models from spatio-temporal observations have already been proposed (Coca and Billings 2001, Mandelj, Grabec and Govekar 2001, Marcos-Nikolaus, Martin-Gonzalez and Sóle 2002, Grabec and Mandeji 1997, Parlitz and Merkwirth 2000). In practice however, some of these approaches may fail to produce models that accurately describe the underlying spatio-temporal patterns either due to an inability to adapt the model structure to that of the unknown system, or because the functions used to implement the model structure are not suitable for modelling the underlying dynamics. This is especially critical when an equivalent description of a real-world system is sought. In such cases the estimated model should provide very accurate information regarding the dynamical properties of the observed system. Theoretical studies have shown that $L^2(R^n)$ can be decomposed into a direct-sum of a family of wavelet subspaces $\{W_i\}_{-\infty}^{\infty}$ in the sense that every $f \in L^2(R^n)$ has a unique wavelet decomposition (Chui 1992). Furthermore, the wavelet representation of any nonlinear function can be shown to be asymptotically near optimal in the sense that the convergence rates are equal to the best attainable using general nonlinear approximation schemes (DeVore, Jawerth, and Popov 1992). Wavelet approximations also provide similar rates of approximation for functions belonging to a wide variety of function spaces including functions with sparse singularities or functions that are not uniformly smooth or regular. All these properties suggest that wavelet multiresolution expansions should provide an excellent foundation for the development of identification algorithms for nonlinear spatio-temporal models.

In this paper an approximated B-spline wavelet representation of spatio-temporal dynamical systems is identified using an orthogonal least squares algorithm (Chen, Billings, and Luo 1989) from measured data. Control variables are incorporated to include controlled external inputs and/or some system parameters for the purpose of analysis. Section 2 introduces the wavelet representation of spatio-temporal dynamical systems. The identification algorithm is given in section 3. Section 4 illustrates the proposed approach using two examples. Finally conclusions are drawn in section 5.

2 Wavelet representations of spatio-temporal dynamical systems

Consider a discrete-time spatio-temporal system defined over a lattice I

$$x_i(t) = f(x_i(t-1), u_i(t-1), \nabla_i(t)) \tag{1}$$

where $x_i(t) \in R$ and $u_i(t) \in R, i \in I$ are the state and input of the system located at site i

at discrete time instant t. $\nabla_i(t)$ denotes spatio-temporal coupling effects for the site i at time instant t from the spatial neighbourhood sites in $\Omega \subset I$ which involve $x_j(t-1)$ and $u_j(t-1)$, $j \in \Omega$. The evolution of the system on the lattice I is governed by the map f, which is generally a nonlinear function. As will be seen in the examples, the input u might be an external controlled signal (Example 1) or a known system parameter (Example 2). The latter case can be interpreted as a technique for obtaining a model with an explicit parameter dependence, based on which the behaviour of the system can be analysed qualitatively.

Let y_i is the observation variable of the system at site i. Assume that the size of the lattice I is finite (this is always the case when a local reconstruction is considered). Then according to the embedding theory (Takens 1981, Sauer, Yorke, and Casdagli 1991, and Casdagli 1992), the system (1) can always be equivalently described as the following input-output form

$$y_i(t) = g(y_i(t-1), \cdots, y_i(t-n_y); u_i(t-1), \cdots, u_i(t-n_u); \nabla_i'(t-1), \cdots, \nabla_i'(t-n_c)) \quad (2)$$

providing n_y, n_u, and n_c are sufficiently large, in which the term ∇_i' denotes the spatio-temporal coupling effects from the spatial neighbourhood sites in $\Omega \subset I$ which involves some delayed values of $y_j(t)$ and $u_j(t)$, $j \in \Omega$.

Given observations of $y(t)$ and the input $u(t)$, the objective of the identification is to approximate the input-output relationship function g in (2) from this data. A practical solution is to approximate the unknown nonlinear function from the available data using a known set of basis functions or regressors belonging to a given function class. Typical regressor classes include polynomials, spline functions, rational functions, radial basis functions, neural networks, and wavelets. In this paper, the algorithm and results for identification using B-spline wavelets are presented.

2.1 B-spline wavelet approximation

The wavelet decomposition of a multivariate function g defined on R^n can be described as follows. Let Φ be a bounded function defined on R^n. For all $p \in Z$ and $k \in Z^n$, a series of functions defined on R^n can be derived in terms of the translates and dyadic dilates of Φ: $\Phi(2^p\mathbf{x} - k)$. Then if $\Phi_{p,k}(x) = \Phi(2^p x - k)$, $p \in Z, k \in Z^n$ form a Riesz basis, function g has a unique decomposition in terms of $\Phi_{p,k}$

$$g(x) = \sum_{p,k} \alpha_{p,k} \Phi_{p,k}(x) \quad (3)$$

Such a Riesz basis in space $L^2(R^n)$ can be constructed from the univariate scaling function ϕ and the associated wavelet function ψ by using the tensor product method. The univariate scaling function considered in this paper is the m-th order cardinal B-spline function $\phi(x) = \phi^m(x) = \beta^m(x)$ given by the recursive relation

$$\beta^m(x) = \frac{x}{m-1}\beta^{m-1}(x) + \frac{m-x}{m-1}\beta^{m-1}(x-1) \tag{4}$$

where $\beta^1(x)$ is the indicator function

$$\beta^1(x) = \begin{cases} 1 & \text{if } x \in (0,1) \\ 0 & \text{otherwise} \end{cases} \tag{5}$$

The wavelet function is defined as a linear combination of scaling functions

$$\psi^m(x) = \sum_{l=0}^{3m-2} q_l^m \phi^m(2x-l) \tag{6}$$

and the coefficients are given by

$$q_l^m = \frac{(-1)^l}{2^{m-1}} \sum_{k=0}^{m} \binom{m}{k} \phi^{2m}(l-k+1),\ l = 0, \cdots .3m-2 \tag{7}$$

If the nonlinear function g in eqn.(2) lies in $L^2(R^n)$, then the B-spline wavelet representation of the input-output equation (2) can be described as follows

$$y_i(t) = \sum_p \sum_k \sum_{l=1}^{2^n-1} \theta_{p,k,l} \Psi_{p,k}^{(l)}(x(t)) \tag{8}$$

where all θ represent parameters and $x(t) = (x_1(t), x_2(t), \cdots, x_n(t))^T$ whose components represent the lagged terms shown in (2), and $\Psi_{p,k}^{(l)}(x)$ are the $2^n - 1$ n-dimensional wavelet functions produced by the tensor product of the univatiate B-spline scaling and wavelet functions ϕ and ψ. According to the multiresolution analysis (Chui 1992), eqn.(8) can equivalently be expressed as

$$y_i(t) = \sum_k \theta_{p_0,k,0} \Phi_{p_0,k}(x(t)) + \sum_{p \geq p_0} \sum_k \sum_{l=1}^{2^n-1} \theta_{p,k,l} \Psi_{p,k}^{(l)}(x(t)) \tag{9}$$

where p_0 is the starting resolution level and Φ is the n-dimensional scaling function.

The wavelet multiresolution approximation (9) is generally an infinite series expansion. In practice, however, it is not realistic to use all the terms in this infinite series expansion. Generally the objective of the identification is to obtain a truncated finite representation containing the terms up to some orders of scaling and dilation. Therefore the identified model will be an approximate representation of the underlying system, which can be equivalently described as an

infinite wavelet series. Alternatively it can be said that the identified model will be a compressed version of the original series expansion. Let s be a positive integer, then the s-truncated space Σ_{s,p_0} with a starting resolution p_0 is the set of all functions

$$h(x) = \sum_k \theta_{p_0,k,0}\Phi_{p_0,k}(x) + \sum_{p_0 \le p \le s} \sum_k \sum_{l=1}^{2^n-1} \theta_{p,k,l}\Psi_{p,k}^{(l)}(x) \tag{10}$$

Note that the series in space Σ_{s,p_0} are those up to dyadic level s, which may possibly be infinite because there is no limitation on the translation operation. In practice, the range of measured data is always finite so that there are only finite numbers of translation operations which produce non-empty intersections within the range of the data because B-spline scaling and wavelet functions have compact supports. Therefore, the identified wavelet series are always finite. Furthermore, in many applications, a 3-truncated space is often enough to obtain a good approximation result for smooth functions. Using the approximation space Σ_{s,p_0} as a regressor class, a truncated approximation representation of (9) takes the form

$$y_i(t) = \sum_k \theta_{p_0,k,0}\Phi_{p_0,k}(x(t)) + \sum_{p_0 \le p \le s} \sum_k \sum_{l=1}^{2^n-1} \theta_{p,k,l}\Psi_{p,k}^{(l)}(x(t)) \tag{11}$$

2.2 An alternative representation of the input-output relationship

For simplicity and without loss of generality, let the nonlinear function to be identified be defined on the cube $[0,1]^n$, and consider the number of wavelet terms in the basis in the space Σ_{s,p_0}. Let $\phi(x)$ and $\psi(x)$ be the univaritate B-spline scaling and wavelet functions of order m. Then the support of $\phi(x)$ and its dilates and translates $\phi_{p,k}(x) = 2^{p/2}\phi(2^p x - k)$ are $[0, m]$ and $[2^{-p}k, 2^{-p}(m+k)]$, and the support of $\psi_{p,k}(x) = 2^{p/2}\psi(2^p x - k)$ are $[0, 2m-1]$ and $[2^{-p}k, 2^{-p}(2m-1+k)]$. Assume that the domain of nonlinear functions to be identified in one component is $[0,1]$, it is then sufficient that the translate parameter k for univariate scaling and wavelet functions falls into the intervals

$$\begin{aligned} \phi &: -m+1 \le k \le 2^p - 1 \\ \psi &: -2(m-1) \le k \le 2^p - 1 \end{aligned} \tag{12}$$

It follows that the total number of terms in the basis of the space Σ_{s,p_0} for n-dimensional functions defined on the cube $[0,1]^n$ is $\sum_{p=p_0}^{s}(n_p)^n$, $n_p = 2^{p+1}+3(m-1)$. For instance, if $n = 6, m = 4, p_0 = 0, s = 1$ which means the dimension of the approximated function is 6 with B-spline scaling and wavelet functions of order 4, starting resolution 0 and the truncation 3, then the total number of the terms in the basis of the space Σ_{s,p_0} is $6,598,370$, which is clearly a time-consuming number for any identification algorithm. To overcome this difficulty, in this paper the identified nonlinear function g is first decomposed into a number of functional components as follows

$$g(x_1,\cdots,x_n) = g_0 + \sum_{i=1}^{n} g_i(x_i) + \sum_{1\le i<j\le n} g_{ij}(x_i,x_j) + \sum_{1\le i<j<k\le n} g_{ijk}(x_i,x_j,x_k) + \cdots + g_{1\cdots n}(x_i,\cdots,x_n) \tag{13}$$

where g_0 is a constant. A truncated representation of (13) containing the functional components up to tri-variate terms is often sufficient to express a nonlinear function itself. Applying the above wavelet decomposition to each of the functional components significantly reduces the number of the terms used for identification. Assume that a multivariate function is defined on $[0,1]^n$ again. Consider the l-variate functional components, the total number of significant terms (the intersection of its support and $[0,1]^n$ is non-empty) can be calculated according to the following formula

$$\binom{n}{l} \sum_{p=p_0}^{s} (n_p)^l, n_p = 2^{p+1} + 3(m-1) \tag{14}$$

Now consider the same example above but with maximal functional components up to the tri-variate case. If $p_0 = 0$, and $s = 2, 1$, and 0 for uni, bi, and tri-variate components, this yields a total of $31,145$ terms. This is a significant reduction compared to $6,598,370$.

3 Identification algorithm

Given a set (candidate terms) of basis functions from the wavelet regressor class, the objective of the identification algorithm is to select the significant terms from this set while estimating the corresponding wavelet coefficients. In this paper, an Orthogonal Forward Regression algorithm (OFR) (Chen, Billings, and Luo 1989) is applied to a set of wavelet basis functions. The OFR algorithm involves a stepwise orthogonalisation of the regressors and a forward selection of the relevant terms based on the Error Reduction Ratio criterion (Billings, Chen, and Kronenberg 1988). The algorithm provides the optimal least-squares estimate of the wavelet coefficients θ.

For a given candidate regressor set $G = \{\varphi_i\}_{i=1}^{M}$, the OFR algorithm can be outlined as follows

Step 1

$$I_1 = I_M = \{1,\cdots,M\}$$

$$w_i(t) = \varphi_i(t), \hat{b}_i = \frac{w_i^T y}{w_i^T w_i} \tag{15}$$

$$l_1 = arg\max_{i\in I_1}(\hat{b}_i^2 \frac{w_i^T y}{y^T y}) = arg\max_{i\in I_1}(err_i) \tag{16}$$

$$w_1^0 = w_{l_1}, c_1^0 = \frac{w_1^{0T} y}{w_1^{0T} w_1^0} \tag{17}$$

$$a_{1,1} = 1 \tag{18}$$

Step $j, j > 1$

$$I_j = I_{j-1} \backslash l_j - 1 \tag{19}$$

$$w_i(t) = \varphi_i(t) - \sum_{k=1}^{j-1} \frac{w_k^{0T} y}{w_k^{0T} w_k^0} w_k^0, \hat{b}_i = \frac{w_i^T y}{w_i^T w_i} \tag{20}$$

$$l_j = arg \max_{i \in I_j} (\hat{b}_i^2 \frac{w_i^T y}{y^T y}) = arg \max_{i \in I_j} (err_i) \tag{21}$$

$$w_j^0 = w_{l_j}, c_j^0 = \frac{w_j^{0T} y}{w_j^{0T} w_j^0} \tag{22}$$

$$a_{k,j} = \frac{w_k^{0T} \varphi_{l_j}}{w_k^{0T} w_k^0}, k = 1, \cdots, j-1. \tag{23}$$

The procedure is terminated at the M_s-th step when the termination criterion

$$1 - \sum_{i=1}^{M_s} err_i < \rho \tag{24}$$

is met, where ρ is a designated error tolerance, or when a given number of terms in the final model is reached.

The estimated wavelet coefficients are calculated from the following equation

$$\begin{pmatrix} \theta_{l_1} \\ \theta_{l_2} \\ \vdots \\ \theta_{l_{M_s}} \end{pmatrix} = \begin{pmatrix} 1 & a_{1,2} & \cdots & a_{1,M_s} \\ 0 & 1 & \vdots & a_{2,M_s} \\ \vdots & \vdots & \ddots & \vdots \\ 0 & 0 & \cdots & 1 \end{pmatrix}^{-1} \begin{pmatrix} c_1^0 \\ c_2^0 \\ \vdots \\ c_{M_s}^0 \end{pmatrix} \tag{25}$$

and the selected terms are $\varphi_{l_1}, \cdots, \varphi_{l_{M_s}}$.

4 Numerical simulation and analysis

4.1 Example 1 - Non-homogeneous wave equation

Consider the following non-homogeneous wave equation (Trim 1990)

$$\frac{\partial^2 y(x,t)}{\partial t^2} = c^2 \frac{\partial^2 y(x,t)}{\partial x^2} + g(x,t), x \in [0, L] \tag{26}$$

with initial conditions

$$\begin{aligned} y(x,0) &= f(x) \\ \frac{dy(x,t)}{dt} &= 0 \end{aligned} \tag{27}$$

and boundary conditions

$$\begin{aligned} y(0,t) &= 0 \\ y(L,t) &= 0 \end{aligned} \tag{28}$$

where

$$g(x,t) = ae^{-x} sin(\omega t) \tag{29}$$

Applying the finite Fourier transform method, the exact solution $y(x,t)$ of the initial boundary value problem (26), (27) and (28) is

$$\begin{aligned} y(x,t) &= \sqrt{\frac{2}{L}} \sum_{n=1}^{\infty} sin(\frac{n\pi x}{L})[\tilde{f}(\lambda_n) cos(c\lambda_n t) + \frac{a\omega sin(c\lambda_n t)}{(\omega^2 - c^2\lambda_n^2)c\lambda_n} \sqrt{\frac{2}{L}} \int_0^L e^{-x} sin(\frac{n\pi x}{L}) dx \\ &\quad - \frac{a sin(\omega t)}{\omega^2 - c^2\lambda_n^2} \sqrt{\frac{2}{L}} \int_0^L e^{-x} sin(\frac{n\pi x}{L}) dx] \end{aligned} \tag{30}$$

where $\lambda_n^2 = n^2\pi^2/L^2$ and $\tilde{f}(\lambda_n) = \int_0^L f(x) sin(n\pi x/L) dx$.

A general wave equation describes the propagation of waves. When c and a are fixed, the waveforms of such a non-homogeneous wave equation depend on the frequency ω of the external input $g(x,t)$. The higher the frequency ω is, the faster the wave propagates.

Terms	Estimates	ERR	STD
$\phi_{0,0}(y_i(t-1))$	5.9835e-01	9.9723e-01	3.1299e-02
$\phi_{0,0}(y_i(t-2))$	-3.7838e-01	2.2570e-03	1.3435e-02
$\phi_{0,0}(u_i(t-1))$	1.4666e-01	5.1896e-05	1.2762e-02
$\phi_{0,0}(y_{i-1}(t-1))$	7.0630e-01	9.4316e-05	1.1409e-02
$\phi_{0,0}(y_{i+1}(t-1))$	5.2912e-01	1.2171e-04	9.3406e-03
$\phi_{0,0}(y_{i+1}(t-2))$	-2.1116e-01	2.0641e-05	8.9455e-03
$\phi_{0,0}(y_{i-1}(t-2))$	-2.9445e-01	1.6902e-05	8.6038e-03
$\phi_{0,0}(u_i(t-2))$	-1.0197e-01	6.6488e-06	8.4664e-03
$\psi_{1,-1}(u_i(t-1))$	1.4838e-02	4.7350e-06	8.3647e-03
$\psi_{0,0}(y_{i-1}(t-1))$	2.4488e-02	4.4949e-06	8.2729e-03
$\psi_{2,2}(y_{i-1}(t-1))$	1.9482e-01	3.3862e-06	8.2002e-03
$\psi_{2,-1}(u_i(t-1))$	-2.4181e-03	2.9021e-06	8.1375e-03
$\psi_{2,-2}(u_i(t-1))$	2.6610e-03	2.8176e-06	8.0759e-03
$\psi_{0,0}(y_i(t-2))$	-2.1334e-02	1.9588e-06	8.0324e-03
$\phi_{2,1}(y_i(t-1))$	-3.3351e-03	1.9571e-06	7.9889e-03

Table 1: Example 1: The terms and parameters of the final CML model

The reason why this simple linear system was chosen for the identification and analysis is because the exact solution can be obtained. Therefore the analysis can be carried out with high confidence. The overall simulation procedure can be divided into two phases: identification and analysis. The identification is conducted by using the proposed wavelet method with a single input frequency ω. Then the obtained model is used to analyse the spatio-temporal patterns under different input frequencies. Note that a discrete version of the form of eqn.(1) for eqn.(26) can be obtained by spatial and time discretisation.

For the purpose of identification using the proposed approach, for a single input frequency $\omega = 1$ the solution (30) with parameters $L = 1$, $f(x) = 0, x \in [0, 1]$, $c = 1$, and $a = 5$ was sampled at 21 equally spaced points over the spatial domain $[0, 1]$. From each location, 300 input/output data points sampled at $\Delta t = 0.1$ were generated. Note that all data were normalised to the interval $[0, 1]$. The data are plotted in Fig.(1).

In this simulation, the neighbourhood was selected to be $i - 1$ and $i + 1$ in the spatial domain and $t - 1, t - 2$ in the time domain. A set of 350 spatio-temporal observations randomly selected among the data set was used for the identification, which is shown in Fig.(2). The identified model using the orthogonal least squares algorithm with the following parameters: order of B-spline 2, initial scale 0, the maximal resolution 2 for all variables and the tolerance 10^{-5}, are listed in Table (1), where ERR denotes the Error Reduction Ratio and STD denotes the standard deviations.

From Table (1), the identified spatio-temporal dynamical model is

$$
\begin{aligned}
y_i(t) = {} & 0.59835\phi_{0,0}(y_i(t-1)) - 0.0033351\phi_{2,1}(y_i(t-1)) - 0.37838\phi_{0,0}(y_i(t-2)) \\
& -0.021334\psi_{0,0}(y_i(t-2)) + 0.14666\phi_{0,0}(u_i(t-1)) - 0.0024181\psi_{2,-1}(u_i(t-1)) \\
& +0.014838\psi_{1,-1}(u_i(t-1)) + 0.0026610\psi_{2,-2}(u_i(t-1)) - 0.10197\phi_{0,0}(u_i(t-2)) \\
& +0.70630\phi_{0,0}(y_{i-1}(t-1)) + 0.024488\psi_{0,0}(y_{i-1}(t-1)) + 0.19482\psi_{2,2}(y_{i-1}(t-1)) \\
& -0.29445\phi_{0,0}(y_{i-1}(t-2)) + 0.52912\phi_{0,0}(y_{i+1}(t-1)) - 0.21116\phi_{0,0}(y_{i+1}(t-2))
\end{aligned} \tag{31}
$$

The model predicted output of the identified model and some snapshots are plotted in Fig.(3) and Fig.(4) respectively. Fig.(5) shows the model predicted error between the exact solution and the identified model predicted output.

The results clearly indicate that the error falls within the amplitude range -0.041902 and 0.050004 and does not grow in time. The root-mean-square (RMS) error is 0.013681. In this example, the obtained CML model can be considered as an estimated and compressed version of the real wavelet representation of the original dynamics. Although there are errors between the real output and the model predicted output it is clearly observed that the identified CML model is able to reproduce the original patterns with high fidelity. Note that model predicted outputs and errors are used here rather than the one-step-ahead predicted outputs. Model predicted outputs represent a much more severe test of model performance compared to one-step-ahead predictions.

The obtained model (31) was used to analyse the spatio-temporal patterns under different input frequencies ω. Figs.(6), (7), (8), and (12) are the actual system output, model predicted output, model predicted error, and some snapshots for the frequency $\omega = 1.5$. Figs.(9), (10), (11), and (13) are the actual system output, model predicted output, model predicted error, and some snapshots for the frequency $\omega = 0.5$. The dependence of the propagation speed on the input frequency can clearly been seen from Figs. (7) and (10). This is consistent with the results from theoretical analysis.

4.2 Example 2 - A CML in a 2-dimensional lattice

Consider the following diffusively coupled map model in a 2-dimensional lattice (Kaneko 1989)

$$
x_{i,j}(t) = (1-\varepsilon)f(x_{i,j}(t-1)) + \frac{\varepsilon}{4}(f(x_{i,j-1}(t-1)) + f(x_{i,j+1}(t-1)) + f(x_{i-1,j}(t-1)) + f(x_{i+1,j}(t-1))) \tag{32}
$$

which $x_{i,j}(t) i, j = 1, \cdots, N$ is the state of the CML located at site (i, j) at discrete time t, ε is the coupling strength, and N is the size of lattice. The evolution of the CML on the lattice sites is governed by the local map f. In this simulation, the mapping function f is chosen as the logistic map

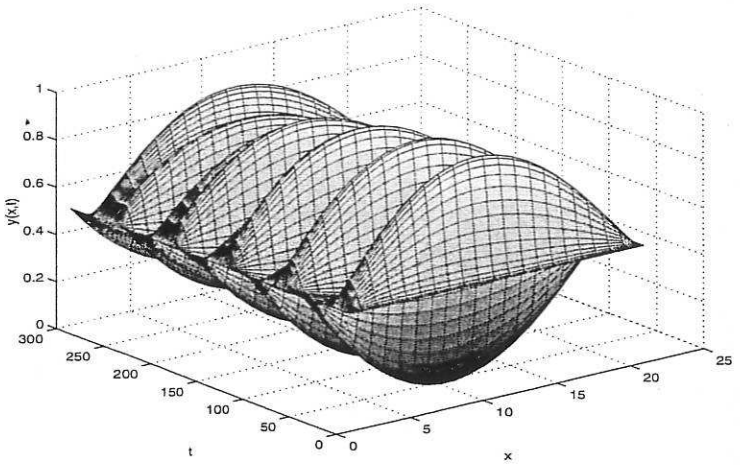

Figure 1: Example 1: System output with frequency $\omega = 1.0$

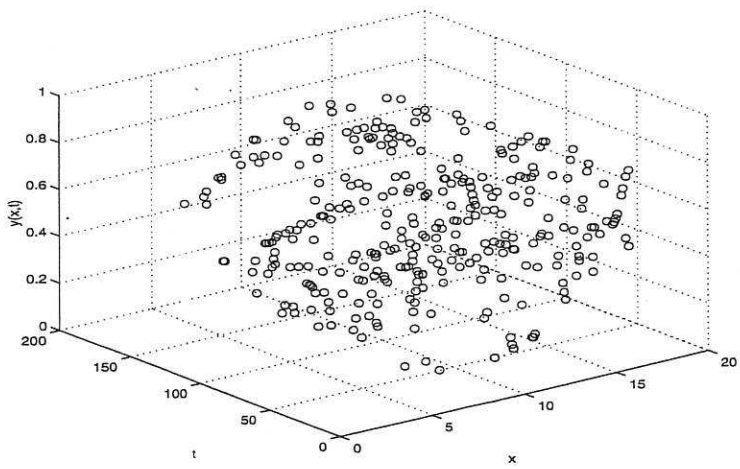

Figure 2: Example 1: The data for identification ($\omega = 1.0$)

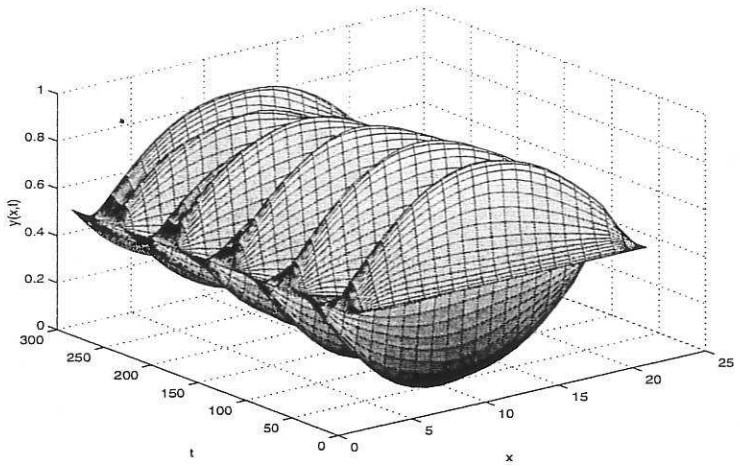

Figure 3: Example 1: Model predicted output with frequency $\omega = 1.0$

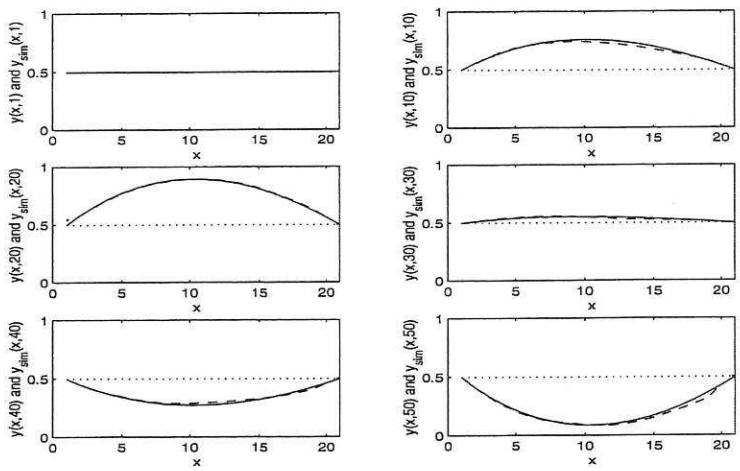

Figure 4: Example 1: Some snapshots of system and model predicted outputs ($\omega = 1.0$)

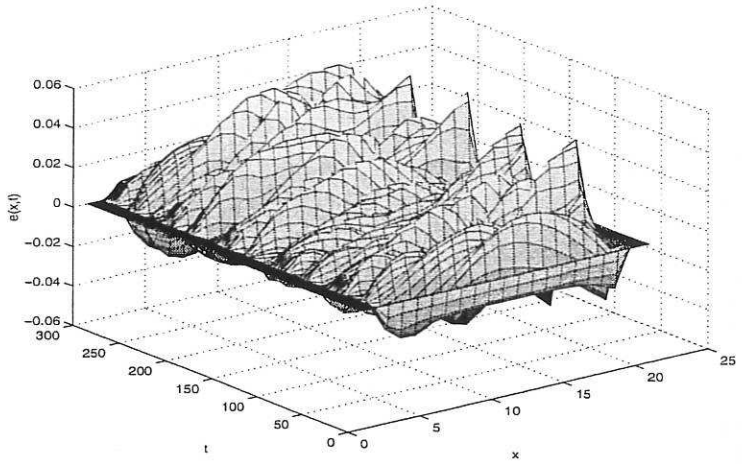

Figure 5: Example 1: Model predicted error ($\omega = 1.0$)

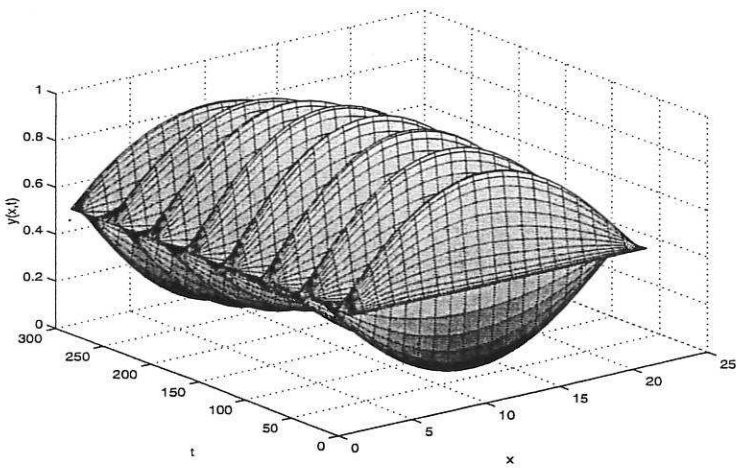

Figure 6: Example 1: System output with frequency $\omega = 1.5$

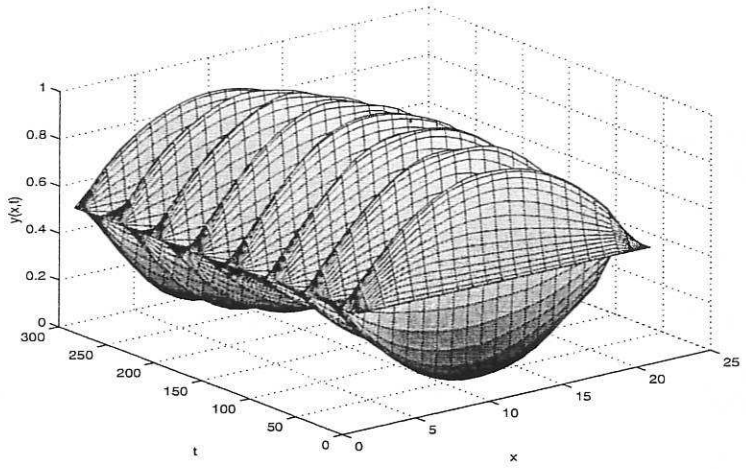

Figure 7: Example 1: Model predicted output with frequency $\omega = 1.5$

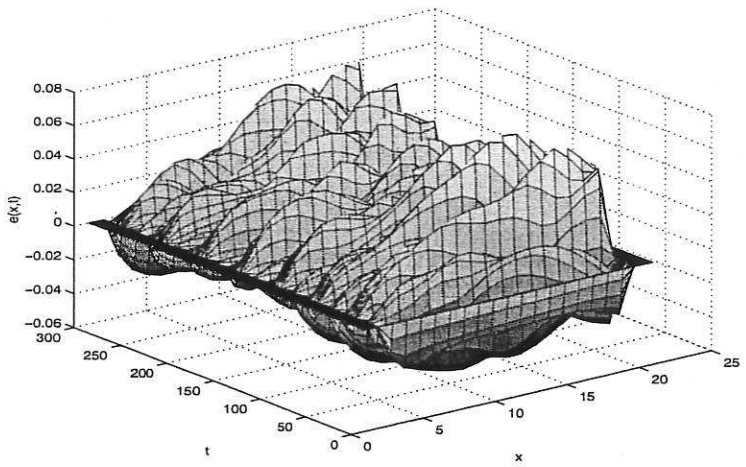

Figure 8: Example 1: Model predicted error ($\omega = 1.5$)

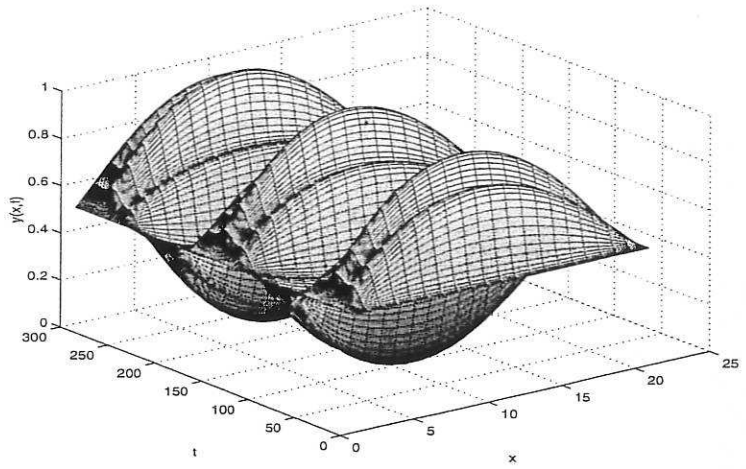

Figure 9: Example 1: System output with frequency $\omega = 0.5$

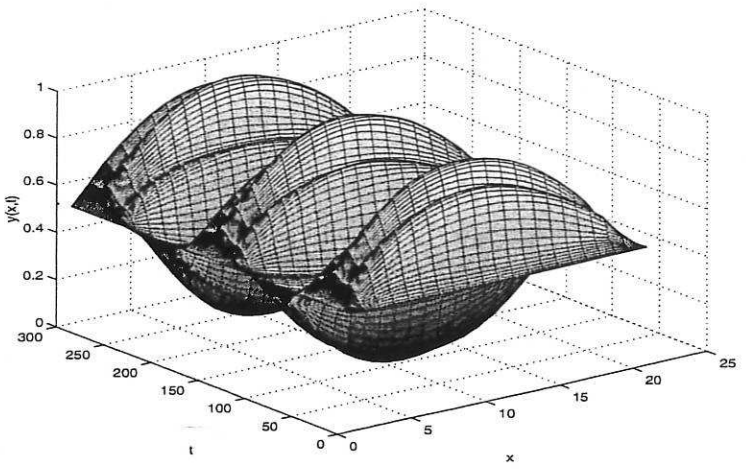

Figure 10: Example 1: Model predicted output with frequency $\omega = 0.5$

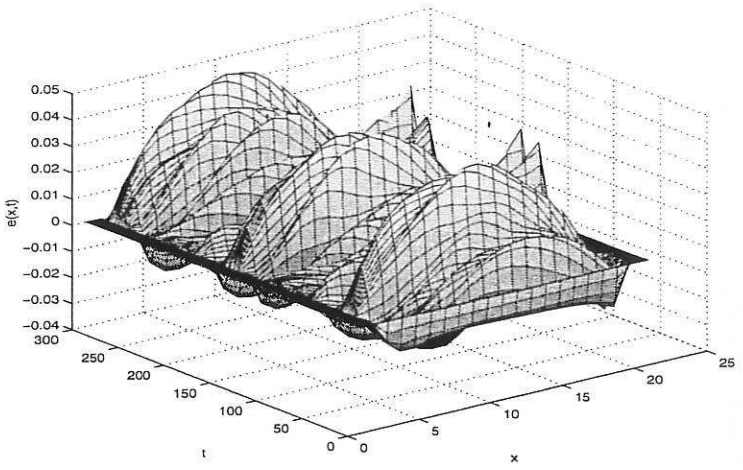

Figure 11: Example 1: Model predicted error ($\omega = 0.5$)

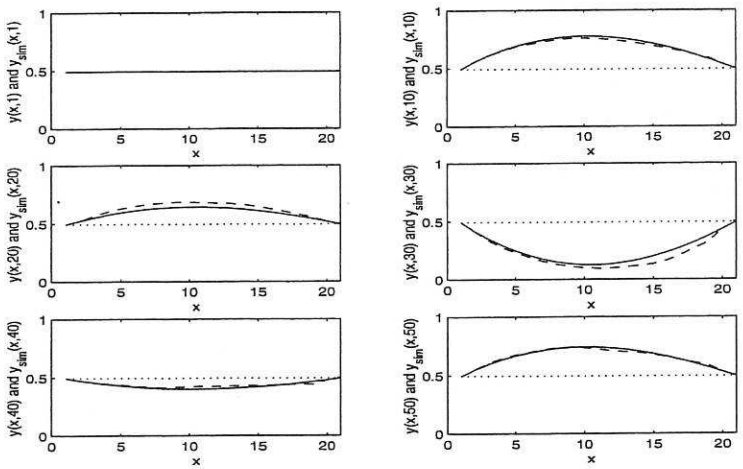

Figure 12: Example 1: Some snapshots of system and model predicted outputs ($\omega = 1.5$)

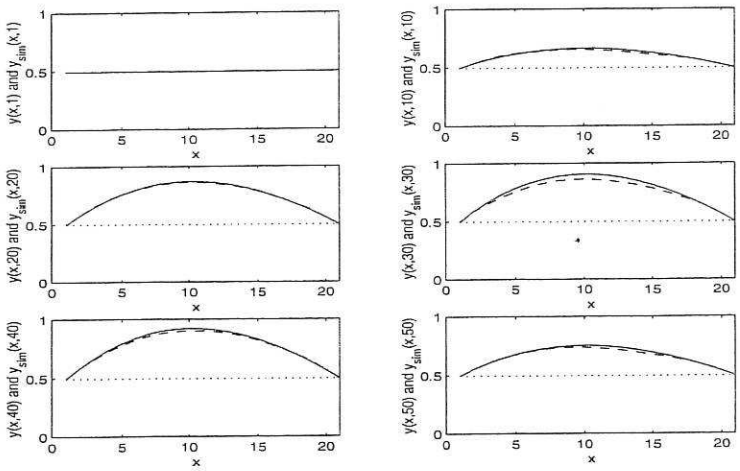

Figure 13: Example 1: Some snapshots of system and model predicted outputs ($\omega = 0.5$)

$$f(x) = 1 - ax^2 \tag{33}$$

Note that the observation variable $y_{i,j}$ was set to be $x_{i,j}$.

This model has been extensively studied. It has been observed that for small $\varepsilon < 0.3$ the system evolves from a frozen random state to pattern selection and to fully developed spatio-temporal chaos via spatio-temporal intermittency. For strong coupling ($\varepsilon > 0.3$) neither a frozen random pattern nor a pattern selection regime is formed. When $\varepsilon > 0.3$ the change of Lyapunov exponents with the parameter a is smooth and the Lyapunov spectra have a smooth shape for all a (Kaneko 1989). Actually in this case a rich set of bifurcations takes place for the logistic map f and $\varepsilon > 0.3$. Fig.(14) shows a bifurcation diagram with $\varepsilon = 0.4$ for $a \in [0.5, 2]$ at the site $(4, 4)$ for a 8×8 lattice. It can be observed that the system is in a stable state for $0.5 \leq a < a_c = 0.741$, period doubling is presented at $a = a_c = 0.741$ and the is followed by quasiperiodic attractors and chaos.

To identify a wavelet model, the data used for identification were generated by simulating the CML model (32) with $\varepsilon = 0.4$ and $a = 1.5$ for 100 steps over a 50×50 lattice I starting from randomly generated initial populations and periodic boundary conditions. The data are shown in Fig.(15). The identification was performed using the proposed method from a set of 100 observation pairs among the data and the four nearest neighbours, namely $(i-1, j), (i+1, j), (i, j-1), (i, j+1)$. Technically, the parameter a was used as a constant external input for this identification. The time lag was set to be 1. The starting resolution was set to be 0 for all variables and the maximal resolutions were set to 2, 1, and 0 for uni, bi, and tri-variates, respectively. The univariate B-spline function of order 3 was used to generate all the higher-dimensional terms by tensor products. It follows that the total number of terms in the set of candidate model set for all two subsystems is 41,809. The identified model is listed in Table (2)

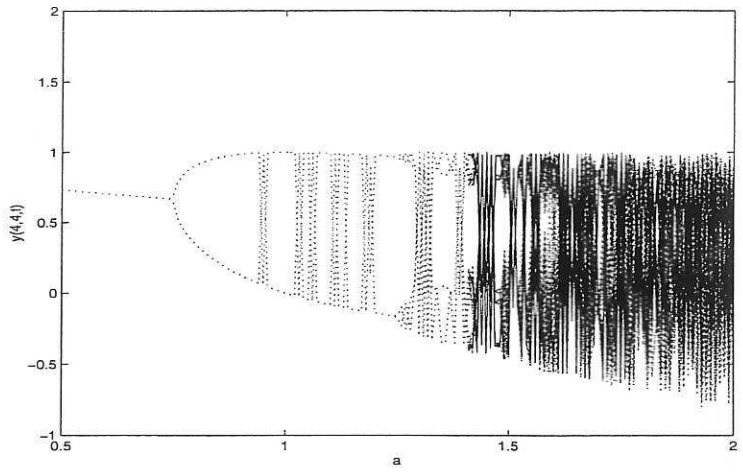

Figure 14: Example 2: Bifurcation diagram for CML model (32)-(33) at spatial site $(4, 4)$ in a 8×8 lattice with random initial conditions

Terms	Estimates	ERR	STD
$\phi_{0,-1}(a)$	7.7332e+00	5.9557e-01	4.0143e-01
$\phi_{0,0}(x_{i,j}(t-1))\phi_{0,0}(a)$	-2.3945e+00	3.9439e-01	6.3269e-02
$\phi_{0,0}(x_{i-1,j}(t-1))\phi_{0,0}(x_{i+1,j}(t-1))$	-1.0176e-02	4.2545e-03	4.8039e-02
$\phi_{0,1}(x_{i,j}(t-1))\phi_{0,0}(x_{i,j-1}(t-1))\phi_{0,0}(x_{i,j+1}(t-1))$	-3.7296e-03	2.2013e-03	3.7824e-02
$\phi_{0,1}(x_{i,j}(t-1))\phi_{0,0}(x_{i-1,j}(t-1))\phi_{0,1}(x_{i+1,j}(t-1))$	-1.3098e-02	7.0021e-04	3.3936e-02
$\phi_{0,1}(x_{i-1,j}(t-1))\phi_{0,0}(x_{i+1,j}(t-1))\phi_{0,0}(a)$	2.0435e-03	7.4365e-04	2.9247e-02
$\phi_{0,1}(x_{i-1,j}(t-1))\phi_{0,0}(a)\psi_{0,1}(x_{i,j-1}(t-1))$	-1.3418e-02	3.6967e-04	2.6610e-02
$\phi_{0,1}(x_{i,j-1}(t-1))\phi_{0,1}(x_{i-1,j}(t-1))\phi_{0,1}(x_{i+1,j}(t-1))$	3.1734e-02	4.2823e-04	2.3183e-02
$\phi_{0,0}(x_{i,j+1}(t-1))$	-2.9840e-01	4.2683e-04	1.9167e-02
$\phi_{0,0}(x_{i,j-1}(t-1))$	-2.8647e-01	2.7855e-04	1.6013e-02
$\psi_{1,3}(x_{i-1,j}(t-1))$	4.1324e-02	1.7249e-04	1.3699e-02
$\phi_{0,0}(x_{i-1,j}(t-1))\phi_{0,0}(a)$	-3.8232e-01	1.1728e-04	1.1872e-02
$\psi_{1,3}(x_{i,j}(t-1))\psi_{1,3}(x_{i+1,j}(t-1))$	-2.7193e-01	1.2565e-04	9.5333e-03
$\phi_{0,0}(x_{i+1,j}(t-1))$	-2.8967e-01	1.0820e-04	6.9117e-03
$\psi_{1,3}(x_{i+1,j}(t-1))$	5.7012e-02	4.3412e-05	5.5204e-03
$\psi_{1,3}(x_{i,j}(t-1))$	8.5030e-02	2.2541e-05	4.6361e-03
$\psi_{2,5}(x_{i-1,j}(t-1))$	-2.7741e+00	1.9594e-05	3.6995e-03
$\psi_{1,2}(x_{i,j+1}(t-1))\psi_{1,3}(x_{i-1,j}(t-1))$	-5.2572e-02	1.2033e-05	2.9820e-03
$\phi_{0,1}(x_{i,j}(t-1))\phi_{0,0}(a)$	3.3401e-02	7.1018e-06	2.4622e-03
$\psi_{1,1}(x_{i,j-1}(t-1))\psi_{1,3}(x_{i,j+1}(t-1))$	-8.4093e-02	4.5755e-06	2.0590e-03

Table 2: Example 2: The terms and parameters of the final CML model

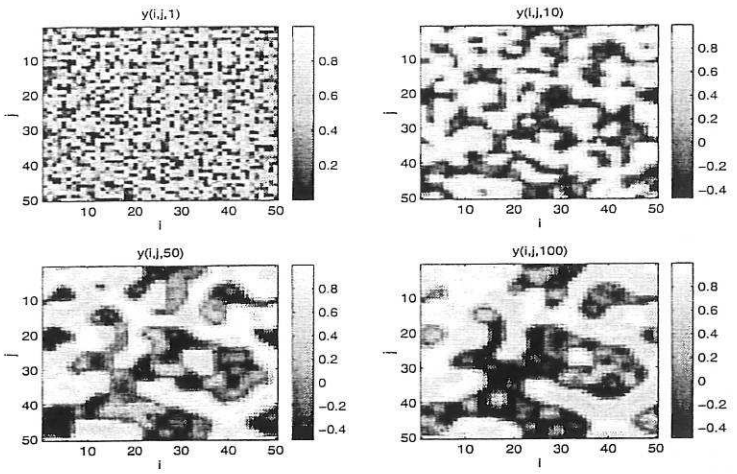

Figure 15: Example 2: Some snapshots of the data

Figs. (16) and (17) show snapshots of the model predicted outputs and errors at time instants $1, 10, 50$ and 100, which show that the identified CML model can reproduce the spatio-temporal patterns of the original system very well.

To analyse the behaviour of the system under different parameters, an estimated bifurcation diagram of the system (32) for the parameter $a \in [0.5, 2]$ at a site $(4, 4)$ for a 8×8 lattice was calculated using the identified model. This bifurcation diagram (Fig.(18)) was drawn using the final 200 data points out of a total 1000 points generated by the identified model. It seems that Fig.(14) and Fig.(18) are quite different. Indeed, on the whole they are different numerically. However the local zoomed diagrams Figs.(19) and (20), and Figs.(21) and (22) show that they are quite similar, in particular in the region around $a = 1.5$ because the model was identified using this value of the parameter. It can also be observed from the estimated bifurcation diagram that the model system is in a stable state for $0.5 \leq a < a_c = 0.741$, period doubling appears at $a = a_c = 0.741$ and is followed by quasiperiodic attractors and chaos. These transition points are almost exactly the same as in the original CML system for $a < 1.85$.

The Lyapunov exponents with $\varepsilon = 0.4, a = 1.55$ were calculated through the product of Jacobians for time steps 1 to 100 for a sub-lattice of the size 3×3 with the site (25, 25) as the centre point, where the boundary effect has been neglected. The values are $\lambda_1 = 0.0648$, $\lambda_2 = 0.0622$, $\lambda_3 = 0.0158$, $\lambda_4 = -0.0014$, $\lambda_5 = -0.0106$, $\lambda_6 = -0.0275$, $\lambda_7 = -0.0478$, $\lambda_8 = -0.0811$, and $\lambda_9 = -0.1360$. It follows that the KS entropy is 0.1428, which is just the sum of all the positive Lyapunov exponents. In order to be able to calculate the largest positive Lyapunov exponent from the data, a numerical algorithm proposed by Rosenstein, Collins, and De Luca (1993) was employed. For the model predicted data from site (25, 25), the slope of the curve obtained by the algorithm was found to converge towards a common value for the choice of embedding dimensions m and provided a value of $\lambda_1 \cong 0.0644$ for the largest Lyapunov exponent which is very close to the value of 0.0648 obtained by the product of Jacobians. The correlation dimension was also estimated by Rosenstein's method to be around 0.495.

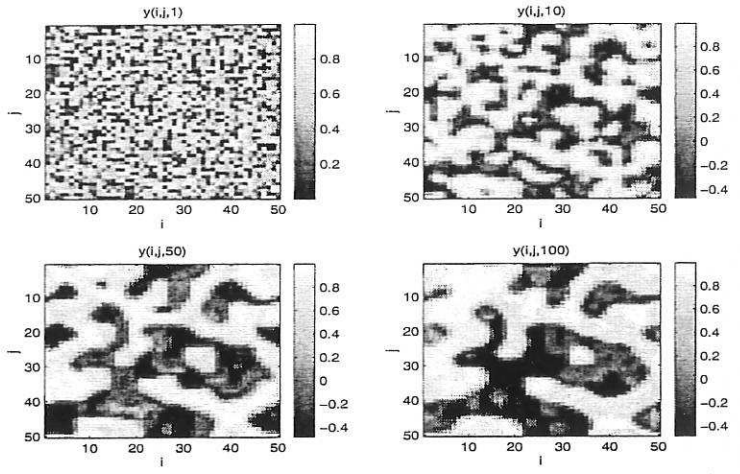

Figure 16: Example 2: Some snapshots of the model predicted output

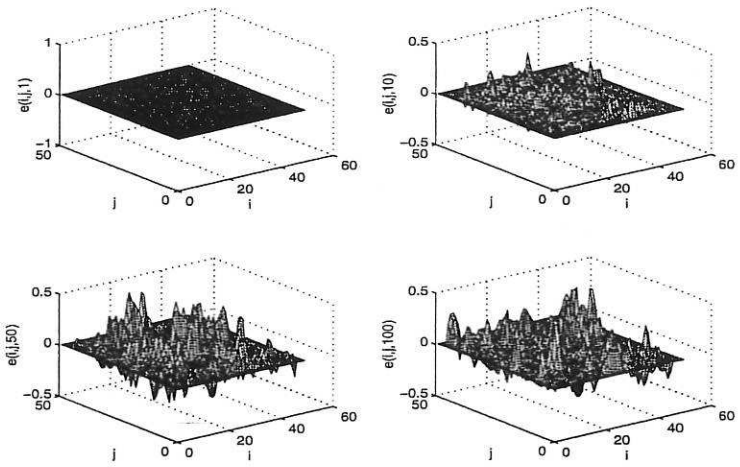

Figure 17: Example 2: Some snapshots of the model predicted error

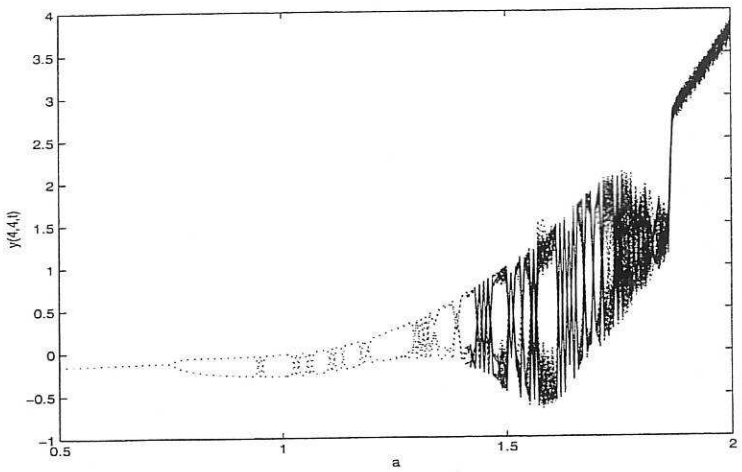

Figure 18: Example 2: Bifurcation diagram of identified model

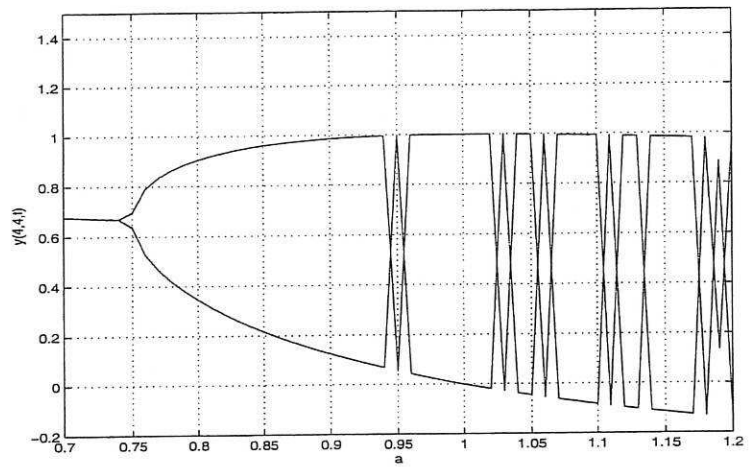

Figure 19: Example 2: Bifurcation diagram of CML model (local)

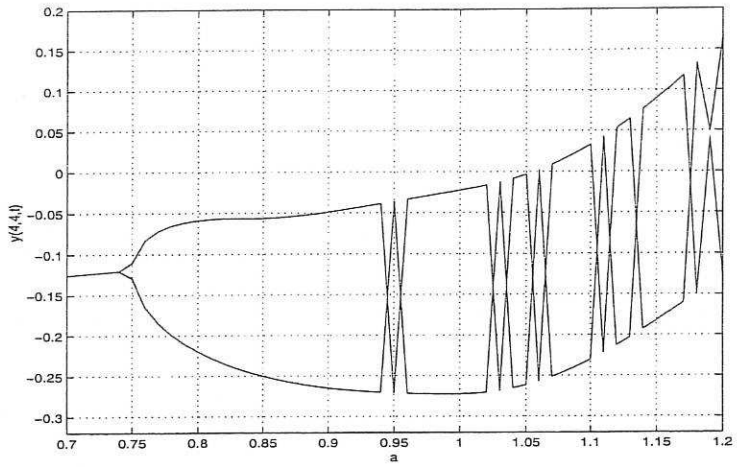

Figure 20: Example 2: Bifurcation diagram of the identified model (local)

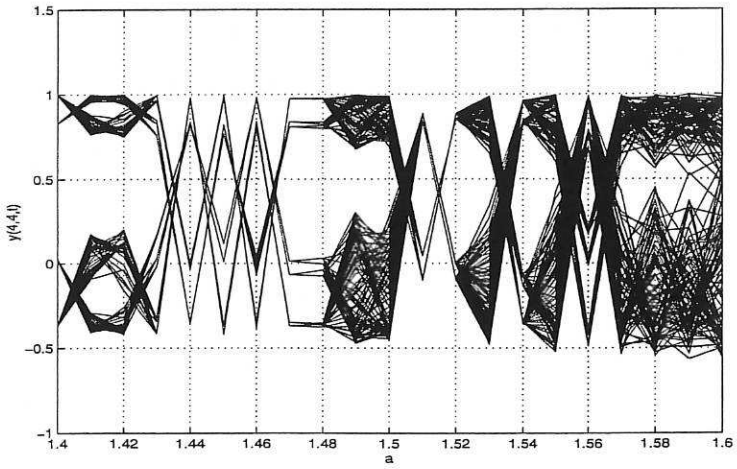

Figure 21: Example 2: Bifurcation diagram of CML model (local)

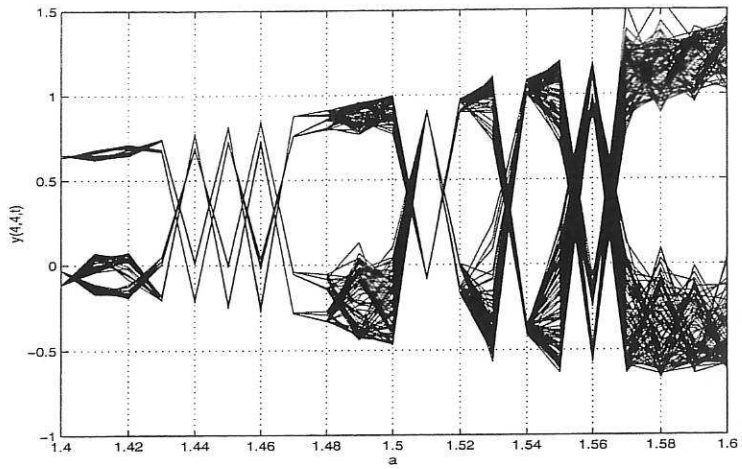

Figure 22: Example 2: Bifurcation diagram of the identified model (local)

5 Conclusions

A new approach for the identification and analysis of spatio-temporal dynamical systems has been introduced. It has been shown that by incorporating a control variable, a spatio-temporal model with explicit external inputs or parameters can be obtained using the proposed method, and that this model can then be used to study pattern formation and system behaviour.

6 Acknowledgement

The authors gratefully acknowledge financial support from EPSRC (UK).

References

[1] Adamatzky, A., (2003) On patterns in affective media, *International Journal of Modern Physics C*, Vol. 14, No. 5.

[2] Bertram, M., Beta, C., Pollmann, M., Mikhailov, A. S., Rotermund, H. H., and Ertl, G., (2003) Pattern formation on the edge of chaos: experiments with CO oxidation on a Pt(110) surface under global delayed feedback, *Phys. Rev.*, E67, No. 3, 036208.

[3] Billings, S. A., Chen, S., and Kronenberg, M. J., (1988) Identification of MIMO nonlinear systems using a forward-regression orthogonal estimator, *Int. J. Contr.*, Vol. 49, pp. 2157-2189.

[4] Casdagli, M., (1992) A dynamical systems approach to modelling input-output systems, in *Nonlinear modelling and forcasting*, Casdagli and Eubank (eds.), Addison-Wesley Publishing Co., pp. 266-281.

[5] Chen, G. (eds.), (1999) *Controlling chaos and bifurcations in engineering systems*, CRC Press, Boca Raton, FL, USA.

[6] Chen,, S., Billings, S. A., and Luo, W., (1989) Orthogonal least squares methods and their application to non-linear system identification, *International Journal of Control*, Vol. 50, No. 5, pp. 1873-1896.

[7] Chui, C. K., (1992) *An introduction to wavelets*, Academic Press, Inc., USA.

[8] Coca, D. and Billings, S. A., (2001) Identification of coupled map lattice models of complex spatio-temporal patterns, *Phys. Lett.*, A287, pp. 65-73.

[9] DeVore, R. A., Jawerth, B., and Popov, V., (1992) Compression of wavelet decompositions, *American Journal of Mathematics*, Vol.114, pp.737-785.

[10] Goldman, D. I., Shattuck, M. D., Sung, J. M., Swift, J. B., and Swinney, H. L., (2003) Lattice dynamics and melting of a nonequilibrium pattern, *Phys. Rev. Lett.*, Vol. 90, No. 10, 104302.

[11] Grabec, I. and Mandelj, S., (1997) Continuation of chaotic fields By RBFNN, in *Biological and Artificial Computation: From Neuroscience to Technology: Proc.*, Mira, J. et al. eds., Lecture Notes in Computer Science, Springer-Verlag, Vol. 1240, pp. 597-606.

[12] Kaneko, K., (1989) Spatiotemporal chaos in one- and two-dimensional coupled map lattices, *Physica*, D37, pp. 60-82.

[13] Kaneko, K. (eds.), (1993) *Coupled map lattice: theory and experiment*, World Scientific, Singapore.

[14] Köhler, P., Reinhard, K., and Huth, A., (2002) Simulating anthropogenic impacts to bird communities in tropical rain forests, *Biological Conservation*, Vol. 108, pp. 35-47.

[15] Mandelj, S., Grabec, I., and Govekar, E, (2001) Statistical approach to modeling of spatiotemporal dynamics, *Int. J. Bifurcation & Chaos*, Vol. 11, No. 11, pp. 2731-2738.

[16] Marcos-Nikolaus, P., Martin-Gonzalez, J. M. and Sóle, R. V., (2002) Spatial forcasting: detecting determinism from single snapshots, *Int. J. Bifurcation and Chaos*, Vol. 12, No. 2, pp. 369-376.

[17] Parlitz, U. and Merkwirth, C., (2000) Prediction of spatiotemporal time series based on reconstructed local states, *Phys. Rev. Lett.* , Vol. 84, No. 9, pp. 2820-2823.

[18] Rosenstein, M. T., Collins, J. J., and De Luca, C. J., (1993) A practical method for calculating largest Lyapunov exponents from small data sets, *Physica*, D65, pp. 117-134.

[19] Sauer, T., Yorke, J. A., and Casdagli, M., (1991) Embedology, *Journal of Statistical Physics*, Vol. 65, pp. 579-616.

[20] Sóle, R. V., Valls, J. and Bascompte, J., (1992) Spiral waves, chaos and multiple attactors in lattice models of interacting populations, *Phys. Lett.*, A166, No. 2, pp. 123-128.

[21] Tabuchi, E., Yakawa, T., Mallick, H., Inubushi, T., Kondoh, T., Ono, T., and Torii, K., (2002) Spatio-temporal dynamics of brain activated regions during drinking behaviour in rats, *Brain Research*, Vol. 951, pp. 270-279.

[22] Takens, F., (1981) Detecting strange attractors in turbulence, in *Lecture Notes in Mathematics*, No. 898, pp. 366-381, Springer-Verlag.

[23] Trim, D. W., (1990) *Applied partial differential equations*, Pws-Kent Publishing Company, Boston.

[24] Yanagita, T. and Kaneko, K, (1997) Modeling and characterisation of cloud dynamics, *Phys. Rev. Lett.*, Vol. 78, No. 22, pp. 4297-4300.